agronomy

MDPI

Article

Investigation of the Detectability of Corn Smut Fungus (*Ustilago maydis* DC. Corda) Infection Based on UAV Multispectral Technology

László Radócz [1], Atala Szabó [1], András Tamás [1], Árpád Illés [1,*], Csaba Bojtor [1], Péter Ragán [1], Attila Vad [2], Adrienn Széles [1], Endre Harsányi [1] and László Radócz [3]

[1] Institute of Land Use, Engineering and Precision Farming Technology, Faculty of Agricultural and Food Sciences and Environmental Management, University of Debrecen, H-4032 Debrecen, Hungary; szelesa@agr.unideb.hu (A.S.)
[2] Institutes for Agricultural Research and Educational Farm (IAREF), Farm and Regional Research Institutes of Debrecen (RID), Experimental Station of Látókép, University of Debrecen, H-4032 Debrecen, Hungary
[3] Institute of Plant Protection, Faculty of Agricultural and Food Sciences and Environmental Management, University of Debrecen, H-4032 Debrecen, Hungary
* Correspondence: illes.arpad@agr.unideb.hu

Abstract: Corn smut fungus (*Ustilago maydis* [DC.] Corda) is a globally widespread pathogen affecting both forage and sweet maize hybrids, with higher significance in sweet maize. Remote sensing technologies demonstrated favorable results for disease monitoring on the field scale. The study focused on the changes in vegetation index (VI) values influenced by the pathogen. In this study, four hybrids, two forage maize and two sweet maize hybrids were examined. Artificial infection was carried out at three different doses: a low (2500 sporidium number/mL), medium (5000 sporidium number/mL) and high dose (10,000 sporidium number/mL) with a non-infected control plot for each hybrid. The experimental plots were monitored using a multispectral UAV sensor of five monochrome channels on three different dates, i.e., 7, 14 and 21 days after infection. Five different indices (NDVI, GNDVI, ENDVI, LCI, and NDRE) were determined in Quantum GIS 3.20. The obtained results demonstrated that the infection had a significant effect on the VI values in sweet maize hybrids. A high-dose infection in the Dessert R 73 hybrid resulted in significantly lower values compared to the non-infected hybrids in three indices (NDVI, LCI and GNDVI). In the case of the NOA hybrids, GNDVI and ENDVI were able to show significant differences between the values of the infection levels.

Keywords: corn smut fungus; disease monitoring; multispectral imaging; remote sensing

Citation: Radócz, L.; Szabó, A.; Tamás, A.; Illés, Á.; Bojtor, C.; Ragán, P.; Vad, A.; Széles, A.; Harsányi, E.; Radócz, L. Investigation of the Detectability of Corn Smut Fungus (*Ustilago maydis* DC. Corda) Infection Based on UAV Multispectral Technology. *Agronomy* **2023**, *13*, 1499. https://doi.org/10.3390/agronomy13061499

Academic Editors: Jinling Zhao and Chuanjian Wang

Received: 11 May 2023
Revised: 24 May 2023
Accepted: 26 May 2023
Published: 30 May 2023

1. Introduction

Maize is one of the most important crops in Hungarian agriculture. In 2021, the maize production area in Hungary was 1,076,061 ha (hectares) [1,2], which is almost one-quarter of the Hungarian arable land. Therefore, experiments and various tests related to maize can potentially be decisive, not only from a scientific aspect but also from an economic point of view. In order to carry out a complex field examination of maize, it is essential to evaluate the optimal level of weather conditions, agrotechnics, sowing time and applied fertilizer [3,4]. The nutrient supply and, more specifically, the amount and quality of nitrogen used are of key importance during plant production [5]. Plant pests can cause significant yield losses; therefore, the planning and implementation of appropriate plant protection procedures is one of the most important factors in plant management [6]. One of the most widespread and well-known pathogens of cultivated maize is the corn smut fungus *Ustilago Maydis* [DC.] CORDA [7]. Pathogens and pests can also cause various symptoms in plants. Changes may appear in the plant tissues, such as the deformation and

discoloration of the leaves, the formation of necrotic spots and the drying and bending of the plants [8].

Remote sensing can be used to monitor and detect various symptoms, especially in the case of diseases and pests causing decreased leaf chlorophyll (Chl) and carotenoid (Car) content, mainly caused by viral, bacterial and fungal infections [9].

Agricultural UAVs (Unmanned Aerial Vehicles) provide new opportunities for pathogen assessment in precision farming [10,11]. These devices can be used in the appropriate environmental conditions [12], making it possible to collect large amounts of data in a cost-effective way [13]. Remote sensing technologies can be divided into three main groups in terms of the observation and detection of plant diseases and pests [9].

The first group includes spectral systems based on VIS-SWIR visible light and near-infrared (e.g., Multispectral, Hyperspectral, RGB and NDVI-NDRE) cameras [14].

The second group involves fluorescent and thermal systems, which are based on different thermal cameras (Thermal Imaging Cameras). This method is also suitable for the presymptom detection of pathogens. For example, Gómez (2014) observed changes in rose leaves 5 days after *Peronospora sparsa* infection, before they even produced visible symptoms [15]. Furthermore, it is also possible to detect apple tree scab, *Venturia inequalis*, before its symptoms appear on the crop [16].

The third is SAR (Synthetic Aperture Radar) LiDAR Light Detection and Ranging Laser-based Remote Sensing in Hungarian. Using these methods, morphological and structural changes mainly caused by pathogenic and harmful organisms can be monitored [9]. Currently, the most common vegetation index is the NDVI (chlorophyll content, biomass, etc.) [17]. The vegetation index (NDVI, GNDVI, NDRE, etc.) values clearly show the health status of the observed plant population since the reflectance of the leaves in the visible spectrum (400–700 nm) is low due to the absorbed photosynthetic pigments (mainly chlorophylls and carotenoids) [17]. The reflectance of a plant in a state of stress increases, which can be easily detected with the appropriate tools, sensor systems and instruments. If the chlorophyll content of a leaf decreases, it can absorb less light, meaning that the reflectance increases in the visible spectra, for example on channel RED, but decreases in the near-infrared NIR [18]. Polischuk et al. (1997) performed measurements based on spectral reflectance for the early diagnosis of disease symptoms. In the case of *Nicotiana debneyi* plants, 10 days after artificial infection with tomato mosaic tobamovirus, the reflectance of the leaves decreased (chlorophyll content (Chl) reduction). However, visually detectable symptoms were observed only 2 weeks after the infection [19]. For example, Kuska (2015) examined the development of powdery mildew with a hyperspectral camera, also based on spectral reflectance. Changes were detected on the leaf surface already on the fourth day after infection before the symptoms on the leaves became visible [20]. A plant under stressful conditions (caused by different biotic or abiotic stressors) reacts with defense mechanisms, such as a decrease in the leaf area index (LAI), a change in the chlorophyll content, or a change in the surface temperature. Thus, the spectral changes that occur differ from the values of healthy, stress-free vegetation [21].

The symptoms of corn smut disease caused by the fungus *Ustilago maydis* [DC.] Corda, which is involved in this study, can affect all parts of the maize plant, including the stem, leaf, cob and crest, and it can also reduce the chlorophyll content [22].

At first, pigment destruction and a yellowish color appear, followed by tissue destruction and the appearance of necrotic spots (leaf color changes) [23,24].

It is important to mention that the pathogen has also an effect on increasing different plant hormones, such as AUXIN and CYTOKININ, [25,26], and also plant stress hormones, which are expressed due to the infection, such as APX, MDA, SOD and POD, are higher in corn smut infected (CSI) plants [27]. The spread and importance of the disease are enhanced by the global warming trend, as it prefers dry, warm conditions [28], which are increasingly typical in Hungary and Central Europe as a region [29].

This paper focuses on the changes caused by the infection of the corn smut fungi and their detectability using measurements based on the VIS-SWIR remote sensing technologies with a multispectral camera system.

2. Materials and Methods

2.1. Study Area

The study site is located in the eastern part of Hungary, in Debrecen. A total of 16 plots were created in the experimental area of the University of Debrecen (47°33′6.52″ N. 21°36′5.59″ E). Two sweet maize and two forage maize hybrids (P 9025, ARMAGNAC) and sweet maize (NOA, DESSERT R 73) were involved in the study, as shown in Figure 1. The sowing date was the same for all four hybrids—29 April 2021. The soil has a pH of 7.46 and Arany's plasticity index is 44. The total soil organic matter content was around 2.4% in the topsoil (0–30 cm). The total amount of water in the 0–100 cm depth was measured before the growing season began (8.3.2021). The average of the total water volume in the wide examined profile (0–100 cm) was 20.02 m/m%. The largest amount (23.42 m/m%) of water was located between 10 and 40 cm depth. In the deeper region (50–100 cm) of the soil, the moisture content was lower (18.6 m/m%) than the soil surface (0–50 cm). The soil samples were dried at 105 Celsius degrees for 5 days in a drying chamber. The data in the weather and soil condition database were measured and collected by the University's own weather station at the experiment site.

Figure 1. University of Debrecen, Böszörményi Street campus experimental station. Experiment area: The plots are the same size, approximately 20 m^2, with randomized placement. The size of the experiment area is 400 m^2. Specifically, 5 m long and 4 m wide. Row spacing is 75 cm, 5 rows in total, 17.5 cm spacing between plants within 1 plot, 142–143 plants sown per plot.

The artificial (*Ustilago Maydis* [DC.] Corda) infection was carried out with three different spore concentrations (spore numbers were 2500/mL, 5000/mL, 10,000/mL and +non-infected control).

The temperature was higher than the average of the last 30 years (19.72 °C). The maximum temperature was higher than 30 °C 19 times between 15.05 and 15.07. Between 06.16 and 06.30, the maximum temperature was above 30 °C every day. The average humidity was low in the middle part of the examination period. After the artificial inoculation of the plants, the relative humidity was higher (70%) than the average of the two-month period (Figures 2 and 3).

During the period of examination, the amount of precipitation was lower than the average of the last 30 years (136.1 mm). The rainfall distribution was not equal between 15.05 and 15.07. The major part of the precipitation was concentrated in the first and the

last part of the examined two months. The total amount of precipitation was 89.1 mm (Figure 4).

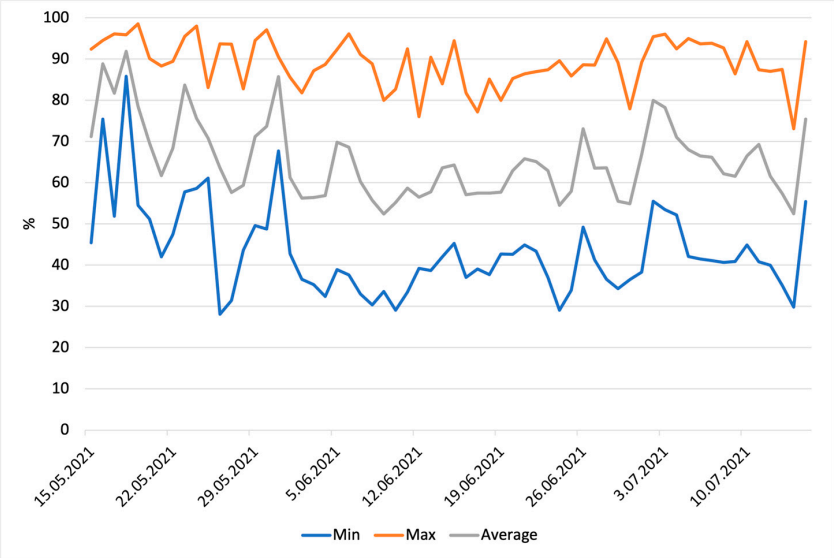

Figure 2. Air humidity in 2021 at the experiment site.

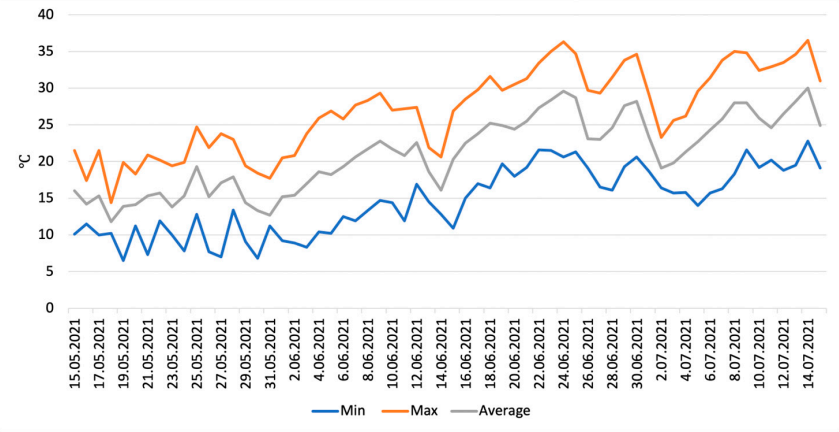

Figure 3. Air temperature in 2021 at the experiment site.

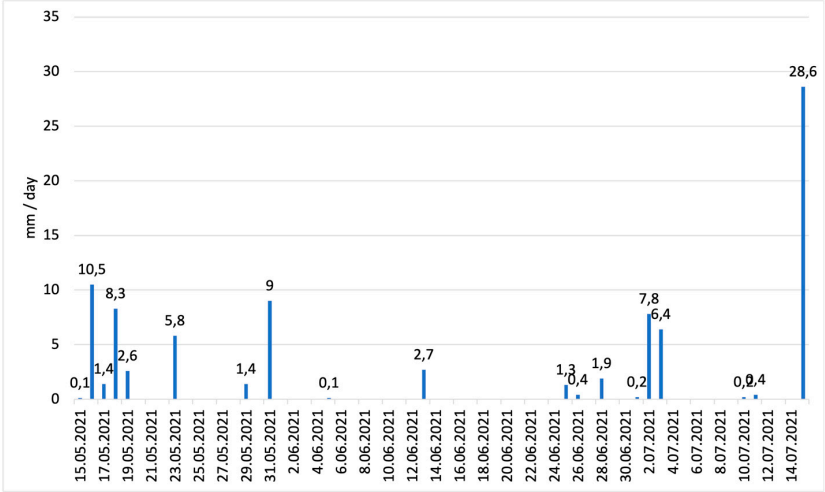

Figure 4. Rainfall in 2021 at the experiment site.

The area was kept weed-free during the tests. Therefore, the values of different weed species could not affect the values on the examined plots. The rows and row spacings were kept clear, and the use of herbicides was avoided. Only mechanical tools were used in this small area.

Three different levels of infection were carried out in the experiment. The plants were treated with the fungus in the 4–5-leaf (V5) phenophase on the 3rd of June. A total of 2 mL of spore suspension was injected into the part of the stem between the second and third node with a mass injection device [27]. The plot IDs and the doses for each plot are shown in Table 1. Cross-infection was not possible in the plots because the reproductive spores of the fungus are formed much later in the vegetative phase, and we observed the earlier stages when only chlorotic changes would appear, and the artificial infection was carried out directly with a suspension produced from compatible fungal strains.

Table 1. The Location of plot IDs and infection levels.

Hybrid	Control	Low Dose	Medium Dose	High Dose
Dessert R 73	4	13	11	6
NOA	16	10	1	7
Armagnac	3	5	14	12
P 9025	9	15	8	2

Artificial infection was performed on 3 June 2021.

- Low concentration: 2500 spores/mL
- Medium concentration: 5000 spores/mL
- High concentration: 10,000 spores/mL

2.2. Experimental Devices and Image Acquisition Methods

The test field was monitored three times during the vegetation period.

The front and side overlap was 80%. The flight altitude was 25 m, with a speed of 3 m/s and a ground sample distance (GSD) of 1.4 cm/px in every case. The total covered area of the flight mission was 0.12 ha and approx. 5 min. for each flight. In order to ensure repeatability, the recordings were always made between 10 am and 11 am. On all three survey dates, the weather was clear and sunny. The capture mode was hover and capture at point. Capture was used by the time interval. Agricultural UAV (drone): DJI Phantom 4 Multispectral RTK drone, which is equipped with a 6-camera Multispectral imaging system 1 visible light and 5 monochrome sensors. FOV (Field of View): 62.7°. Focal Length: 5.74 mm (35 mm format equivalent: 40 mm), autofocus set at ∞. Aperture: f/2.2 [30]. The camera can take 6 pictures simultaneously on 5 different channels. Band 1 is Red (R) 650 nm ± 16 nm, Band 2 is Green (G) 560 nm ± 16 nm, Band 3 is Blue (B) 450 nm ± 16 nm, Band 4 is Red Edge (RE) 730 nm ± 16 nm and Band 5 is Near-Infra RED (NIR) and captures at 840 nm ± 26 nm wavelengths. For each camera sensor, the effective pixels were 2.02 MP (2.12 in total), and the cameras were equipped with a global shutter and a 3-axis gimbal stabilizer [30]. The UAV control software used was DJ GS Pro on IOS with an iPad Mini.

WebODM, the software used in the analysis and evaluation process, is a free application that was used for UAV image processing. Georeferenced maps, point clouds and textured 3D models can be created from aerial photographs (WebODM) [31].

High-resolution orthomosaics were created from the field captures (high-resolution HR 2 cm/pixel). We used these orthomosaics for further QGIS analysis (The imagery was orthorectified using WebODM). Orthophotos were taken on the 5 different channels (Red R, Green G, Blue B, Near-infrared NIR, Red edge RE) on each survey date 7 days (10 June), 14 days (17 June) and 21 days (24 June) following the infection period.

The digitization footprint and sizes of the captured images are presented in Table 2 (raw image format and post-processed Tiff).

Table 2. The digitization footprint of the experiment.

Date	Overlap Front/Side	GSD	Number of Captured Channels	Size in Mb (Raw)	Size in Mb (Tiff)
7 DAI	80%	1.4 cm/px	6	1640	84.7
14 DAI	80%	1.4 cm/px	6	1250	97.1
21 DAI	80%	1.4 cm/px	6	1620	80.6

Quantum GIS 3.20 was used to create and evaluate the different vegetation index (VI) maps (Figure 5). The vegetation index maps were prepared with the raster analysis function and formulas shown in Table 3 (NDVI, NDRE, GNDVI, LCI and ENDVI).

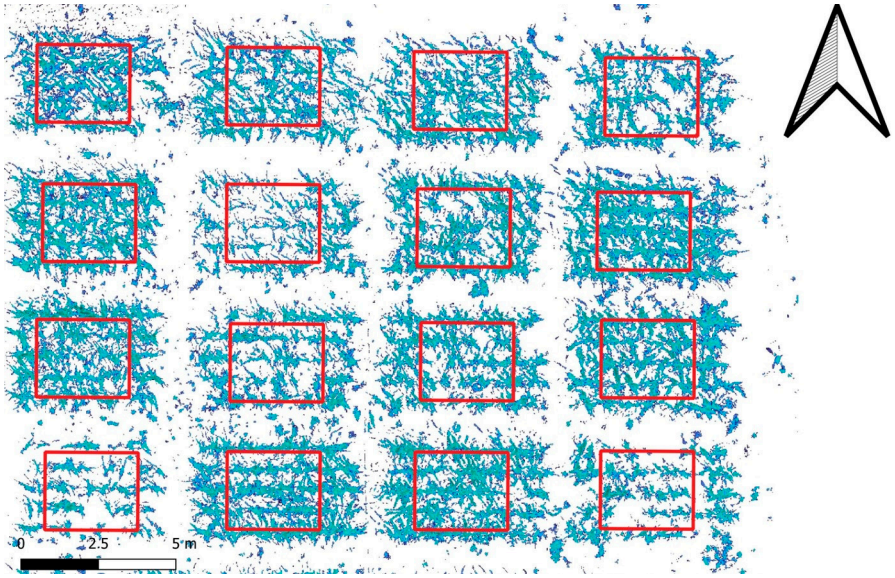

Figure 5. Example of the maps that were created in QGIS 3.20 visualization. NDVI filtered map HR high resolution 2 cm/px containing only maize pixels separated from the background.

Table 3. Vegetation index formulas used in the study.

Abbrev.	Formula	Reference
NDVI	$(R_{NIR} - R_{Red})/(R_{NIR} + R_{Red})$	[32]
GNDVI	$(R_{NIR} - R_{Green})/(R_{NIR} + R_{Green})$	[33]
NDRE	$(R_{NIR} - R_{RedEdge})/(R_{NIR} + R_{RedEdge})$	[34]
LCI	$(R_{NIR} - R_{RedEdge})/(R_{NIR} + R_{Red})$	[35,36]
ENDVI	$(R_{NIR} + R_{Green} - 2 \times R_{Blue})/(R_{NIR} + R_{Green} + 2 \times R_{Blue})$	[37]

In each case, a mask file was created for extracting the maize pixels separated from the background and values of the soils and shadow, i.e., only maize plant pixels were used for further analysis.

Sample values were collected for all the vegetation index maps (ENDVI, LCI, NDRE, etc.) based on the method shown in Figure 6. Each sample box was a 3 × 2.5 m rectangle that covered a multipolygon shape file (Shp) area (NDVI sampling spot). Following the principle of unification, the sample values for each map were collected from the same area.

Guan S. et al. (2019) also collected the sample NDVI values with this method in their experiment [38]. Using these data, statistical mean values were obtained in MS Excel.

Further statistical analyses were performed in R 4.1.2. [39] using the RStudio [40] graphic interface and the "agricolae" [41] packages.

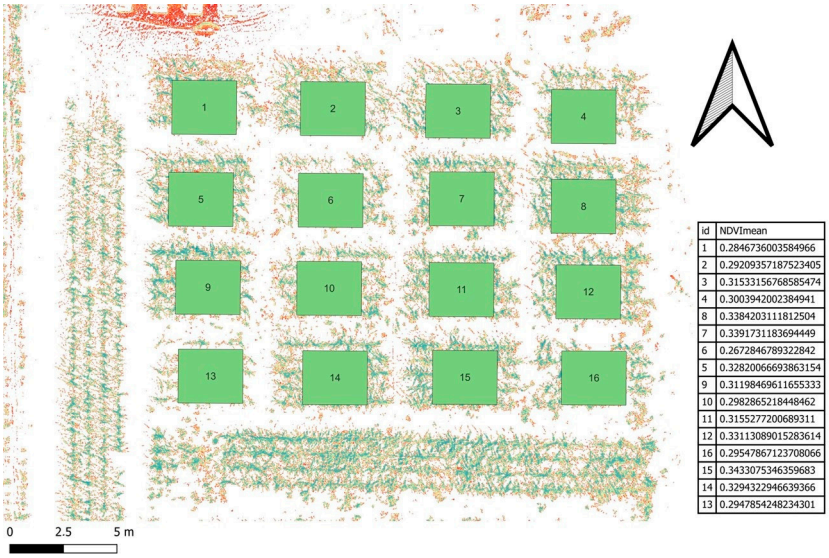

id	NDVImean
1	0.2846736003584966
2	0.29209357187523405
3	0.31533156768585474
4	0.3003942002384941
8	0.33842031111812504
7	0.3391731183694449
6	0.2672846789322842
5	0.32820066693863154
9	0.31198469611655333
10	0.2982865218448462
11	0.3155277200689311
12	0.33113089015283614
16	0.29547867123708066
15	0.3433075346359683
14	0.3294322946639366
13	0.2947854248234301

Figure 6. Sample data collection method. Placement of the experimental area and sampling boxes on the plots, as well as the attribute table of average values from the zonal statistics (NDVI map).

The figures and graphs were created in MS Excel 2016. Based on the example of Huzsvai [42], the repeated measures ANOVA (RMA) model was used to examine the effect of the recording method, dates and infection level and their combined effect, as well as their impact on the vegetation index value changes during the first three weeks of the infection period. The same model was used in each VI map in the case of NDVI, GNDVI, NDRE, LCI and ENDVI and also for each hybrid.

3. Results

The symptoms were fully visible on the experiment field by the third week. The symptoms of the stem (tumors) and leaf corn smut infection were also identified, i.e., discolored brown spots with a yellowish border, necrotic tissues and structural destruction were visible on the surface of the leaves, as shown in Figure 7.

Figure 7. Appearance of visible symptoms (leaf symptom and stalk tumors of *Ustilago maydis* [DC.] Corda) in the treated plots. Third week after infection (21 DAI).

The first recordings were performed 1 week after infection (7 DAI), the second were performed 14 days after infection (14 DAI) and the third were carried out 21 days (DAI) after infection.

The forage maize hybrids P 9025 and Armagnac were more tolerant to the infection than the sweet maize hybrids Dessert R 73 and NOA, as shown also via the symptoms in the field.

The Dessert R 73 results revealed three VIs with a significant effect of the infection, based on the values in Table 4.

Table 4. Significant effect on the values of infection in different VIs in the case of the D73 hybrid.

Infection D73	Df	Sum Sq	Mean Sq	F Value	Pr (>F)
LCI	3	0.0030246	0.0010082	21,059	0.00138 **
NDVI	3	0.003874	0.0012913	7.927	0.0165 *
GNDVI	3	0.010228	0.003409	15.61	0.00307 **

Note: ** indicates that the infection had a significant impact on the values at the 0.01 level; * indicates that the impact was significant at the 0.05 level.

3.1. Results of the Sweet Maize Hybrid Dessert R 73

As shown in the values of the Dessert R 73 hybrid in Table 4, in the case of three VI NDVI, LC, and GNDVI of the five calculated indices, the infection affected the values at various levels.

Based on Figure 8, the values of the control plot had the highest NDVI values at 0.3052, and the values of the plot with a high spore concentration (High 10,000) were the lowest at 0.2560.

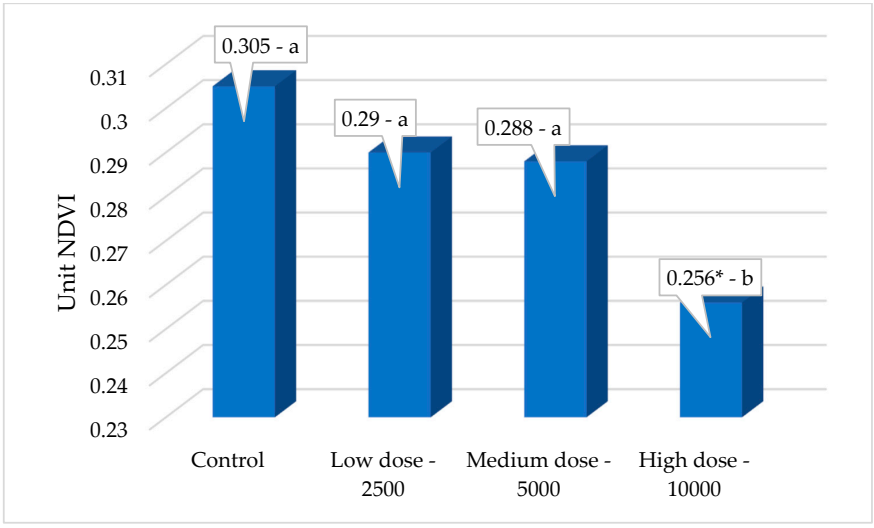

Figure 8. Dessert R 73 Results of NDVI values. Lower case letters (a, b) show the significant differences among treatments based on the ANOVA test ($p < 0.05$). Asterisks mark significant differences compared to control. * $p < 0.05$.

The values of the low-dose plot were 0.2907 (Low 2500), and the values of the plot treated with a medium dose (Medium 5000) showed an NDVI value of 0.2886.

The results of the control plot produced higher values than those of the Low 2500 and Medium 5000 plots. However, they did not differ significantly from each other, and all three belong to Group (a). Based on the NDVI results, the control plot (a) is statistically different from the High 10,000 values (b).

In the case of the high concentration dose 10,000 (b) plot, the NDVI values are lower than both the two treatments and the uninfected control plot. The values of High 10,000 (b) are significantly different from the NDVI values of the other treated plots.

Based on Figure 9, the values of the control plot were the highest with a GNDVI value of 0.2576, and the lowest GNDVI values of the plot with a high spore concentration (High 10,000) were 0.1813.

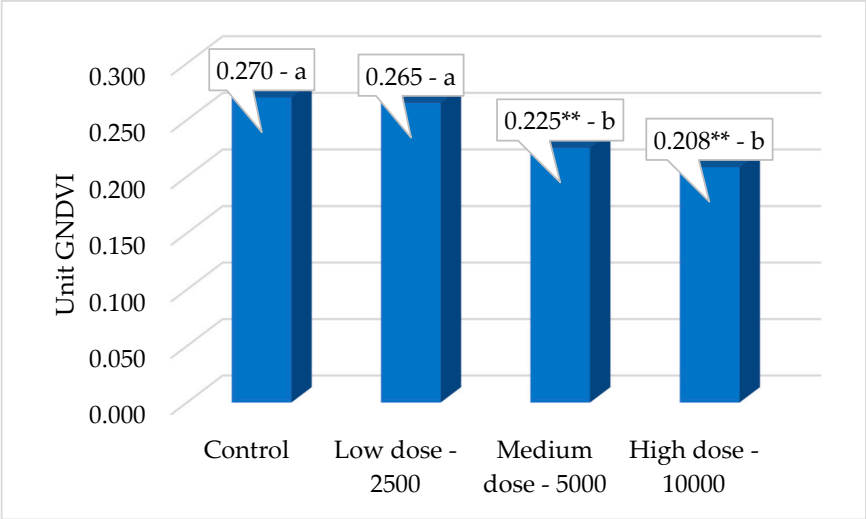

Figure 9. Dessert R 73 results of GNDVI values. Lower case letters (a, b) show the significant differences among treatments based on the ANOVA test ($p < 0.05$). Asterisks mark significant differences compared to control. ** $p < 0.01$. The values of the medium dose plot were 0.2095 (Medium 5000), and the values of the plot treated with a low dose (Low 2500) were 0.2400 GNDVI.

The results of the control plot showed higher GNDVI values than the Low 2500, Medium 5000 and High 10,000 plots and were significantly different from the Medium 5000 (b) and the High 10,000 (b). The Control (a) plot was not significantly different from Low 2500 (a).

In the case of the High 10,000 (b) plot, the GNDVI values were lower than both the two treatments and the uninfected control plot. The values of High 10,000 (b) were significantly different from the GNDVI values of Low 2500 (a) and Control (a). The values of the High 10,000 (b) plot were not significantly different from those of the Medium 2500 (b).

Based on Figure 10, the values of the control plot were the highest with an LCI value of 0.1102, and the values of the plot with a high spore concentration (High 10,000) showed the lowest value of 0.07137.

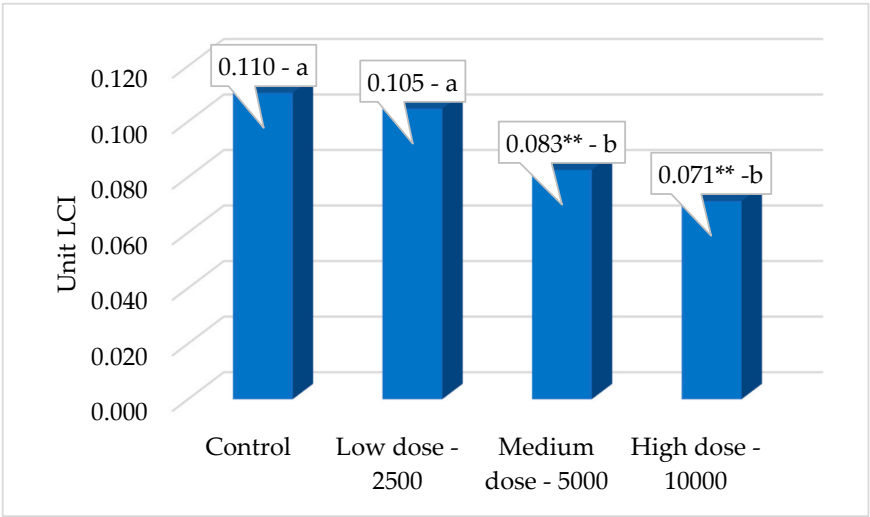

Figure 10. Dessert R 73 results of LCI values. Lower case letters (a, b) show the significant differences among treatments based on the ANOVA test ($p < 0.05$). Asterisks mark significant differences compared to control. ** $p < 0.01$.

The values of the medium dose plot were 0.08258 (Medium 5000), and the values of the low dose treated plot (Low 2500) showed an LCI value of 0.1046.

The results of the control plot showed higher values than the Low 2500 and Medium 5000 plots and also the High 10,000 plot and were significantly different from the Medium 5000 (b) and the High 10,000 (b). The Control (a) plot was not significantly different from the Low 2500 (a).

In the case of the High 10,000 (b) concentration plot, the LCI values were lower than both the two treatments and the uninfected control plot. The values of High 10,000 (b) were significantly different from the LCI values of Low 2500 (a) and Control (a). The values of the High 10,000 (b) plot were not significantly different from those of the Medium 5000 concentration (b).

3.2. Results of the Sweet Maize Hybrid NOA

Based on Figure 11, the values of the control plot were the highest with an ENDVI value of 0.335286, and the values of the plot with a high spore concentration (High 10,000) showed the lowest value of 0.266592. The F value wad 9.173 for the ENDVI, and 11.78 for the GNDV (Table 5).

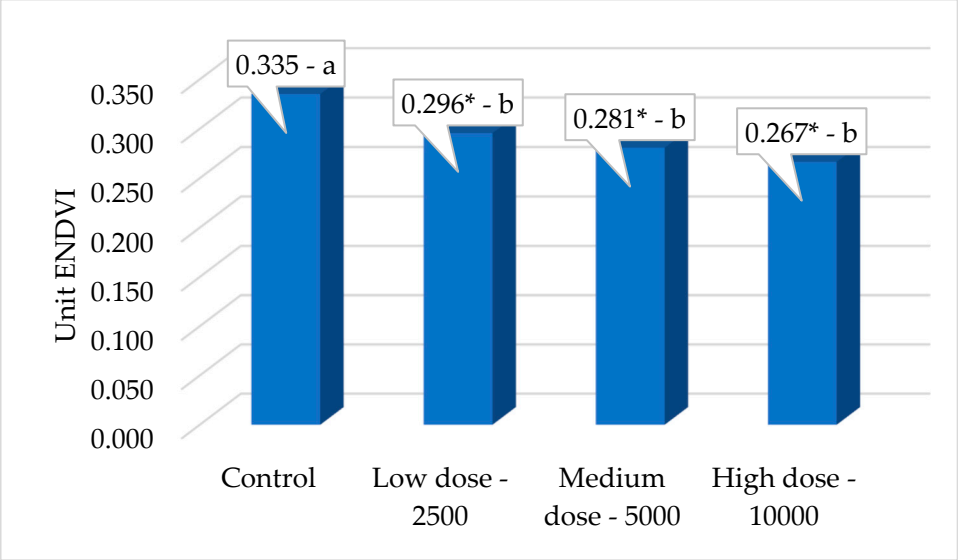

Figure 11. NOA results of ENDVI values. Lower case letters (a, b) show the significant differences among treatments based on the ANOVA test ($p < 0.05$). Asterisks mark significant differences compared to control. * $p < 0.05$.

Table 5. Significant effect on the values of infection in different VIs in the case of the hybrid NOA.

Infection NOA	Df	Sum Sq	Mean Sq	F Value	Pr (>F)
ENDVI	3	0.007891	0.002630	9.73	0.01167 *
GNDVI	3	0.008164	0.002721	11.78	0.00631 **

Note: ** indicates that the infection had a significant impact on the values at the 0.01 level; * indicates that the impact was significant at the 0.05 level.

The values of the medium dose plot were 0.295733 (Medium 5000), and the values of the low dose treated plot (Low 2500) showed an ENDVI value of 0.280846.

The results of the control plot showed higher values than the Low 2500 (b) and Medium 5000 (b) plots and the High 10,000 (b) plot and were significantly different from these three.

In the case of the NOA ENDVI maps, the Medium 5000 (b) was higher than the Low 2500 (b) concentration plot values but was not significantly different.

Based on Figure 12, the values of the control plot were the highest with a GNDVI value of 0.269864, and the values of the plot with a high spore concentration (High 10,000) showed the lowest value of 0.208266.

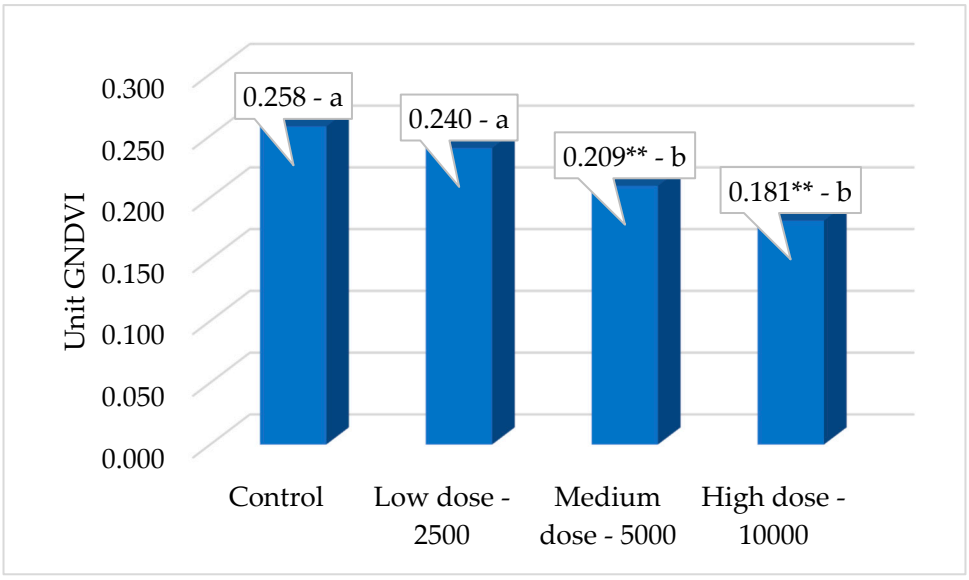

Figure 12. NOA results of GNDVI values. Lower case letters (a, b) show the significant differences among treatments based on the ANOVA test ($p < 0.05$). Asterisks mark significant differences compared to control. ** $p < 0.01$. The values of the medium dose plot were 0.225392 (Medium 5000), and the values of the low dose treated plot (Low 2500) showed an ENDVI value of 0.265049.

The results of the control plot produced higher values than the Low 2500 (a) and Medium 5000 (b) plots and the High 10,000 (b) plot and were significantly different from these two groups.

A summary of the results is shown in Table 6.

Table 6. Summary table of the results.

Infection D73	Control	Low Dose	Medium Dose	High Dose	Pr (>F)
LCI **	0.110 a	0.105 a	0.083 b	0.071 b	0.00138 **
NDVI *	0.305 a	0.290 a	0.288 a	0.256 b	0.0165 *
GNDVI **	0.270 a	0.265 a	0.225 b	0.208 b	0.00307 **
Infection NOA	**Control**	**Low Dose**	**Medium Dose**	**High Dose**	**Pr (>F)**
ENDVI *	0.335 a	0.296 b	0.281 b	0.267 b	0.01167 *
GNDVI **	0.258 a	0.240 b	0.209 b	0.181 b	0.00631 **

Groups marked with different letters are significantly different from each other. Alpha: 0.05 Significant levels * $p < 0.05$, ** $p < 0.01$—the marked results is had significant effect).

4. Discussion

The basis of this VIS-SWIR remote sensing technology method lies in the spectral response of plants under different stress factors. Crops that are affected by different diseases show changes in water content, cell structure, pigment synthesis and colorization of the green parts. In this study, four different hybrids were observed: two forage maize hybrids (P 9025 and Armagnac) and two sweet maize hybrids (Dessert R 73 and NOA). In the case of the forage maize hybrids, there were changes in the VI values, but no significant difference was detected between those indices. It is commonly known that forage maize hybrids are much more resilient against smut fungus but are not fully resistant. In the case of the sweet maize hybrid, previous studies showed that after 11 DACSI (days after corn smut infection), the photosynthetic pigments in the plants were significantly reduced [27]. Chlorosis is one of the most typical symptoms of corn smut fungus [22].

Garcia-Ruiz, F. et al. (2013) investigated HLB-infected citrus trees in Florida. They used multispectral images for the detection and classification. The study included seven vegetation indices, and two indices used in this study (NDVI and GNDVI) were also observed for plant pathogen diagnostic purposes.

Their results showed that the AIV (average index values) of the NDVI and GNDVI in the case of HLB-infected trees were both lower than those of the healthy plants. HLB also affected the leaf's photosynthetic pigments, such as chlorophyll and carotenoids. Similar results were observed in this study. In the case of the plots that were infected with the high (10.000) concentration compared to the healthy plots, the average VI values of the infected plots were significantly lower [43].

De Castro et al. (2015) focused on the early detection of laurel wilt disease in avocado plants. For the purpose of evaluation and analysis, multispectral images were taken, and different VIs were calculated. Spectral data analysis showed significant differences between healthy and LW-infected plants in different infection stages. The GNDVI was an optimal vegetation index for this type of survey based on their results [44].

Albetis J. et al. also used the NDVI and GNDVI in their study for the detection of *Flavescence dorée* in red and white grapevine cultivars. The NDVI and GNDVI were also important variables in their multivariate classification and measuring methods [45].

Gennaro and S.F.D monitored grapevine leaf stripe disease (GLSD) with a multispectral UAV. Their results showed that the GLSD grapevine disease affected the values of the NDVI compared to the healthy plants. They also confirmed that GLSD significantly influenced the NDVI values [46].

Abdulridha et al. extracted vegetation indices from hyperspectral images (UAV-based) to detect tomato diseases. According to the authors, they were able to detect bacterial spots in every stage of the disease development using NDVI (850) [47].

Based on the works of Kaur R. et al., the LCI (Leaf Chlorophyll Index) showed $R^2 = 0.73$ regression with chlorophyll content in wheat [48]. In this experiment, in the case of the Dessert R 73 hybrid, the LCI values were able to detect the effect of the corn smut infection, *Ustilago maydis* [DC.] Corda. The plots that were treated with the highest 10.000 spore concentration showed significantly lower values than the healthy ones.

It was detected that the infection had an impact on the values during the infection period. The field was monitored on three different dates 7 days after the infection (7 DAI), 14 days after infection (14 DAI) and 21 days (21 DAI) after infection.

Orthomosaics were created in WebODM with a high spatial resolution (2 cm/pixel). Using raster analysis, five different VIs were calculated (NDVI, GNDVI, ENDVI, NDRE and LCI). Using Quantum GIS 3.20, in addition to creating maps, sample data were also collected with the sample box method, i.e., a rectangle polygon shape file with the same parameters for all the plots. After acquiring the zonal statistics from all the VI maps, a database was created. Statistical analysis was performed in RStudio 4.1.2 [39] with the RStudio [40] graphic interface using the "agricolae" [41] packages.

The figures and graphs were created in Microsoft Excel 2016. Based on the example of Huzsvai [42], a repeated measures ANOVA (RMA) model was used to examine the effect of the recording method and infection level and their combined effect, as well as their impact on the vegetation index value changes.

In the case of the Dessert R 73 hybrid, three different VIs showed that the infection had affected the obtained values, GNDVI, NDVI and LCI. These three VIs performed well based on the study results.

In the case of the NOA sweet maize hybrid, two VIs showed the effect of the corn smut infection (GNDVI and ENDVI).

5. Conclusions

The novelty of our study is that the obtained results show that the GNDVI showed an outstanding performance in the case of the corn smut fungus *Ustilago maydis* [DC.] Corda monitoring. It was shown that the infection had a significant impact on the values

at the 0.01 ** level in the two sweet maize hybrids, NOA and Dessert R 73. The NDVI, LCI and ENDVI also showed great results regarding tracking the pathogen *Ustilago maydis* [DC.]. These two hybrids are very popular in the Hungarian sweet maize market, so all research and economic studies are relevant for our producers and also for our researchers. This method can be used to detect the changes in different VIs during the period of infection with the modified RMA model. As the concentration was increased, the values became lower in the plots treated with the fungi, and the dynamic changes were evident. With this survey and sample collection method, the sample values from the VIs can be analyzed and evaluated and can be adopted in every other culture. It is possible to investigate different biotic or abiotic stressors on a field scale. The results showed that the dynamics of the values changed over time and were significantly affected by the different infection levels, i.e., field validation is still required in every case, and the values of severity scales should be determined after evaluation, depending on the culture, vegetation period and on-site validation. In addition, using this multispectral device, which is available on the market, experimental sites or fields can be observed in high quality.

Author Contributions: L.R. (László Radócz 1), data curation, writing of the manuscript and performing measurements; C.B. and A.S. (Adrienn Széles), formal analysis, methodology and conceptualization; A.T. and E.H., writing—review and editing; L.R. (László Radócz 2). and P.R., formal analysis; A.T., A.V. and A.S. (Atala Szabó), supervision and review and editing; Á.I., project administration, corresponding author and review of the manuscript. All authors have read and agreed to the published version of the manuscript.

Funding: Project no. TKP2021-NKTA-32 has been implemented with the support provided by the Ministry of Innovation and Technology of Hungary from the National Research, Development and Innovation Fund, financed under the TKP2021-NKTA funding scheme.

Institutional Review Board Statement: Not applicable.

Informed Consent Statement: Not applicable.

Data Availability Statement: All the data supporting the conclusions of this article are included in this article.

Conflicts of Interest: The authors declare no conflict of interest.

References

1. Available online: https://www.ksh.hu/docs/hun/xftp/stattukor/vet/20210601/index.html (accessed on 25 January 2023).
2. Széles, A.; Kovács, K.; Ferencsik, S. The effect of crop years and nitrogen basal and top dressing on the yield of different maize genotypes and marginal revenue. *Időjárás/Q. J. Hung. Meteorol. Serv.* **2019**, *123*, 265–278. [CrossRef]
3. Széles, A.; Harsányi, E.; Kith, K.; Nagy, J. The effect of fertilisation and weather extremities caused by climate change on maize (*Zea mays* L.) yield in Hungary. *J. Agric. Food Dev.* **2018**, *4*, 1–9. [CrossRef]
4. Széles, A.; Ragán, P.; Nagy, J. Abiotic stress impacts caused by weather and nutrient replenishment on the yield of maize (*Zea mays* L). *Columella: J. Agric. Environ. Sci.* **2017**, *4*, 39–44.
5. Rácz, D.; Szőke, L.; Tóth, B.; Kovács, B.; Horváth, É.; Zagyi, P.; Duzs, L.; Széles, A. Examination of the Productivity and Physiological Responses of Maize (*Zea mays* L.) to Nitrapyrin and Foliar Fertilizer Treatments. *Plants* **2021**, *10*, 2426. [CrossRef]
6. Oerke, E.C. Crop losses to pests. *J. Agric. Sci.* **2006**, *144*, 31–43. [CrossRef]
7. Christensen, J.J. *Corn Smut Caused by Ustilago Maydis*; Monographs; American Phytopathology Society: Worcester, MA, USA, 1963; Volume 2.
8. Cao, X.; Luo, Y.; Zhou, Y.; Duan, X.; Cheng, D. Detection of powdery mildew in two winter wheat cultivars using canopy hyperspectral reflectance. *Crop Prot.* **2013**, *45*, 124–131. [CrossRef]
9. Zhang, J.; Huang, Y.; Pu, R.; Gonzalez-Moreno, P.; Yuan, L.; Wu, K.; Huang, W. Monitoring plant diseases and pests through remote sensing technology: A review. *Comput. Electron. Agric.* **2019**, *165*, 104943. [CrossRef]
10. Su, J.; Liu, C.; Hu, X.; Xu, X.; Guo, L.; Chen, W.H. Spatio-temporal monitoring of wheat yellow rust using UAV multispectral imagery. *Comput. Electron. Agric.* **2019**, *167*, 105035. [CrossRef]
11. Su, J.; Liu, C.; Coombes, M.; Hu, X.; Wang, C.; Xu, X.; Chen, W.H. Wheat yellow rust monitoring by learning from multispectral UAV aerial imagery. *Comput. Electron. Agric.* **2018**, *155*, 157–166. [CrossRef]
12. Calou, V.B.C.; dos Santos Teixeira, A.; Moreira, L.C.J.; Lima, C.S.; de Oliveira, J.B.; de Oliveira, M.R.R. The use of UAVs in monitoring yellow sigatoka in banana. *Biosyst. Eng.* **2020**, *193*, 115–125. [CrossRef]

13. Ye, H.; Huang, W.; Huang, S.; Cui, B.; Dong, Y.; Guo, A.; Ren, Y.; Jin, Y. Recognition of banana fusarium wilt based on UAV remote sensing. *Remote Sens.* **2020**, *12*, 938. [CrossRef]
14. Sankaran, S.; Mishra, A.; Ehsani, R.; Davis, C. A review of advanced techniques for detecting plant diseases. *Comput. Electron. Agric.* **2010**, *72*, 1–13. [CrossRef]
15. Gómez Caro, S. Infection and Spread of *Peronospora sparsa* on *Rosa* sp. (Berk.). Ph.D. Thesis, Universitäts und Landesbibliothek Bonn, Bonn, Germany, 2014.
16. Oerke, E.C.; Froehling, P.; Steiner, U. Thermographic assessment of scab disease on apple leaves. *Precis. Agric.* **2011**, *12*, 699–715. [CrossRef]
17. Penuelas, J.; Filella, I. Visible and near-infrared reflectance techniques for diagnosing plant physiological status. *Trends Plant Sci.* **1998**, *3*, 151–156. [CrossRef]
18. Sishodia, R.P.; Ray, R.L.; Singh, S.K. Applications of remote sensing in precision agriculture: A review. *Remote Sens.* **2020**, *12*, 3136. [CrossRef]
19. Polischuk, V.P.; Shadchina, T.M.; Kompanetz, T.I.; Bi, G.; Sozinov, A.L. Changes in reflectance spectrum characteristic of Nicotiana debneyi plant under the influence of viral infection. *Arch. Phytopathol. Plant Prot.* **1997**, *31*, 115–119. [CrossRef]
20. Kuska, M.; Wahabzada, M.; Leucker, M.; Dehne, H.W.; Kersting, K.; Oerke, E.C.; Steiner, U.; Mahlein, A.K. Hyperspectral phenotyping on the microscopic scale: Towards automated characterization of plant-pathogen interactions. *Plant Methods* **2015**, *11*, 28. [CrossRef]
21. Martinelli, F.; Scalenghe, R.; Davino, S.; Panno, S.; Scuderi, G.; Ruisi, P.; Villa, P.; Stroppiana, D.; Boschetti, M.; Goulart, L.R.; et al. Advanced methods of plant disease detection. A review. *Agron. Sustain. Dev.* **2015**, *35*, 1–25. [CrossRef]
22. Snetselaar, K.M.; Mims, C.W. Light and electron microscopy of Ustilago maydis hyphae in maize. *Mycol. Res.* **1994**, *98*, 347–355. [CrossRef]
23. Frommer, D.; Veres, S.; Radócz, L. Susceptibility of stem infected sweet corn hybrids to common smut disease. *Acta Agrar. Debr.* **2018**, *74*, 55–57. [CrossRef]
24. Morrison, E.N.; Emery, R.J.N.; Saville, B.J. Fungal derived cytokinins are necessary for normal Ustilago maydis infection of maize. *Plant Pathol.* **2017**, *66*, 726–742. [CrossRef]
25. Mills, L.J.; Vanstaden, J. Extraction of cytokinins from maize, smut tumors of maize and Ustilago maydis cultures. *Physiol. Plant Pathol.* **1978**, *13*, 73–80. [CrossRef]
26. Turian, G.; Hamilton, R.H. Chemical detection of 3-indolylacetic acid in Ustilago zeae tumors. *Biochim. Biophy. Acta* **1960**, *41*, 148–150. [CrossRef] [PubMed]
27. Szőke, L.; Moloi, M.J.; Kovács, G.E.; Biró, G.; Radócz, L.; Hájos, M.T.; Kovács, B.; Rácz, D.; Danter, M.; Tóth, B. The application of phytohormones as biostimulants in corn smut infected Hungarian sweet and fodder corn hybrids. *Plants* **2021**, *10*, 1822. [CrossRef]
28. Moura, R.M.; Pedrosa, E.M.; Guimarães, L.M. A rare syndrome of corn smut. *Fitopatol. Bras.* **2001**, *26*, 782. [CrossRef]
29. Király, G.; Rizzo, G.; Tóth, J. Transition to Organic Farming: A Case from Hungary. *Agronomy* **2022**, *12*, 2435. [CrossRef]
30. Available online: https://www.dji.com/hu/p4-multispectral/specs (accessed on 25 January 2023).
31. Available online: https://opendronemap.org/webodm (accessed on 25 January 2023).
32. Tucker, C.J. Red and photographic infrared linear combinations for monitoring vegetation. *Remote Sens. Environ.* **1979**, *8*, 127–150. [CrossRef]
33. Gitelson, A.A.; Merzlyak, M.N. Remote sensing of chlorophyll concentration in higher plant leaves. *Adv. Space Res.* **1998**, *22*, 689–692. [CrossRef]
34. Barnes, E.M.; Clarke, T.R.; Richards, S.E.; Colaizzi, P.D.; Haberland, J.; Kostrzewski, M.; Waller, P.; Choi, C.; Riley, E.; Thompson, T. Coincident detection of crop water stress, nitrogen status and canopy density using ground based multispectral data. In Proceedings of the 5th International Conference on Precision Agriculture and Other Resource Management, Bloomington, MN, USA, 16–19 July 2000.
35. Datt, B. A new reflectance index for remote sensing of chlorophyll content in higher plants: Tests using Eucalyptus leaves. *J. Plant. Physiol.* **1999**, *154*, 30–36. [CrossRef]
36. Thenkabail, P.S.; Smith, R.B.; De Pauw, E. Hyperspectral vegetation indices and their relationships with agricultural crop characteristics. *Remote Sens. Environ.* **2000**, *71*, 158–182. [CrossRef]
37. Rasmussen, J.; Ntakos, G.; Nielsen, J.; Svensgaard, J.; Poulsen, R.N.; Christensen, S. Are vegetation indices derived from consumer-grade cameras mounted on UAVs sufficiently reliable for assessing experimental plots? *Eur. J. Agron.* **2016**, *74*, 75–92. [CrossRef]
38. Guan, S.; Fukami, K.; Matsunaka, H.; Okami, M.; Tanaka, R.; Nakano, H.; Sakai, T.; Nakano, K.; Ohdan, H.; Takahashi, K. Assessing correlation of high-resolution NDVI with fertilizer application level and yield of rice and wheat crops using small UAVs. *Remote Sens.* **2019**, *11*, 112. [CrossRef]
39. R Core Team. *R: A Language and Environment for Statistical Computing*; R Foundation for Statistical Computing: Vienna, Austria, 2022. Available online: http://www.R-project.org/ (accessed on 25 January 2023).
40. RSTUDIO Team. *RStudio: Integrated Development for R*; RStudio, Inc.: Boston, MA, USA, 2022. Available online: http://www.rstudio.com/ (accessed on 25 January 2023).

41. De Mendinburu, F.; Agricolae: Statistical Procedures for Agricultural Research. R Package Version 1. 3-5. 2021. Available online: http://CRAN.R-project.org/package=agricolae (accessed on 25 January 2023).
42. Huzsvai, L.; Balogh, P. Lineáris Modellek az R-ben. Seneca Books, Debrecen. 109–124. 2015. Available online: http://seneca-books.hu/doc/Linearis_modellek.pdf (accessed on 25 January 2023).
43. Garcia-Ruiz, F.; Sankaran, S.; Maja, J.M.; Lee, W.S.; Rasmussen, J.; Ehsani, R. Comparison of two aerial imaging platforms for identification of Huanglongbing-infected citrus trees. *Comput. Electron. Agric.* **2013**, *91*, 106–115. [CrossRef]
44. De Castro, A.I.; Ehsani, R.; Ploetz, R.; Crane, J.H.; Abdulridha, J. Optimum spectral and geometric parameters for early detection of laurel wilt disease in avocado. *Remote Sens. Environ.* **2015**, *171*, 33–44. [CrossRef]
45. Albetis, J.; Duthoit, S.; Guttler, F.; Jacquin, A.; Goulard, M.; Poilvé, H.; Féret, J.-B.; Dedieu, G. Detection of Flavescence dorée grapevine disease using unmanned aerial vehicle (UAV) multispectral imagery. *Remote Sens.* **2017**, *9*, 308. [CrossRef]
46. Di Gennaro, S.F.; Battiston, E.; Di Marco, S.; Facini, O.; Matese, A.; Nocentini, M.; Palliotti, A.; Mugnai, L. Unmanned Aerial Vehicle (UAV)-based remote sensing to monitor grapevine leaf stripe disease within a vineyard affected by esca complex. *Phytopathol. Mediterr.* **2016**, *55*, 262–275.
47. Abdulridha, J.; Ampatzidis, Y.; Kakarla, S.C.; Roberts, P. Detection of target spot and bacterial spot diseases in tomato using UAV-based and benchtop-based hyperspectral imaging techniques. *Precis. Agric.* **2020**, *21*, 955–978. [CrossRef]
48. Kaur, R.; Singh, B.; Singh, M.; Thind, S.K. Hyperspectral indices, correlation and regression models for estimating growth parameters of wheat genotypes. *J. Indian Soc. Remote Sens.* **2015**, *43*, 551–558. [CrossRef]